# Influence of ferroelectric layer on artificial multiferroic LSMO/BTO bilayers deposited by DC and RF sputtering

J.E. Ordoñez[a], M.E. Gómez[a,b], and W. Lopera[a]
[a]*Department of Physics, Universidad del Valle, A.A. 25360, Cali, Colombia.*
[b]*Center of Excellence for Novel Materials-CENM, www.cenm.org, Cali, Colombia.*

Received 29 March 2016; accepted 26 July 2016

$La_{2/3}Sr_{1/3}MnO_3$ (LSMO)/$BaTiO_3$ (BTO) bilayers were deposited on (001) $SrTiO_3$ substrates via DC and RF sputtering at pure oxygen atmosphere at a substrate temperature of 830°C. We studied the structural, electrical and magnetic properties on LSMO/BTO bilayers, when LSMO thickness is fixed at 40 nm and BTO thickness is varied from 20 to 100 nm. Reciprocal Space Maps in LSMO show a strained growth for all samples, while BTO layers are always relaxed. Magnetization and electrical measurements indicate the influence of the ferroelectric layer, due to saturation magnetization increases from 500 to 590 emu/cm$^3$ and coercive field decreases from 178 to 82 Oe with BTO thickness. Mean Field mechanism is identified on all samples with critical exponent $\beta$ between 0.42 and 0.54. Resistivity measurements show electron-electron and magnon- magnon scattering conduction mechanisms. The influence on magnetic and electrical properties of bilayers with BTO thickness is attributed to crystallographic strains at the interface and the corresponding relaxation with increasing BTO layer thickness.

*Keywords:* Ferroelectric films; magnetic multilayers; magnetic properties.

PACS: 75.40.Cx; 75.47.Lx; 75.70.Ak.

## 1. Introduction

Fabrication of artificial multiferroic thin film structures, in which ferromagnetic (FM) and ferroelectric (FE) compounds are artificially assembled is valuable, because these structures are promising candidates in exploration of robust cross-coupling effects at room temperature by exploiting the elastic coupling between the two constituents, leading to extrinsic magnetoelectric (ME) effects or other phenomena such as the sheet resistance modulation (Mott transition) in a ferroelectric field-effect transistor (FE-FET) structure, which is comparatively easy to produce as it does not require large defect-free ferroelectric layers [1]. Furthermore, some manganites used like electrodes are known to drastically decrease fatigue on capacitive structures based on $Pb(Zr,Ti)O_3$ - PZT, making them natural candidates for robust FE-FETs [1]. Among the most attractive materials for practical implementation of multiferroic heterostructures and fundamental studies of magnetoelectric coupling are the lanthanum doped manganites, $La_{1-x}A_xMnO_3$, (A=Ca, Sr, or Ba) for FM materials [2], while that for FE material are $BiFeO_3$, $BaTiO_3$ and PZT [3-8]. At ferromagnetic/insulator interfaces, the ME effect may originate from purely electronic mechanisms. It was predicted that displacements of atoms at the FM/FE interface caused by ferroelectric instability alter the overlap between atomic orbitals at the interface, which affects the interface magnetization [9]. This produces a ME effect that manifests itself in the abrupt change in the interface magnetization caused by ferroelectric switching under influence of applied electric field [10]. Additionally, the stacking of layers of different ferroelectrics in a multilayer composite configuration has proven successful for the improvement of the dielectric and ferroelectric properties of single phase films. Some examples are the solid solution $_{(1-x)}(Bi_{0.5}Na_{0.5})TiO_{(3-x)}BaTiO_3$ (BNBT) has been presented as a very promising candidate [11,12]. It shows large piezoelectric coefficients for compositions in the vicinity of a MPB. Recently, it has been reported relaxor-ferroelectric character in the operties of this solid solution for compositions close to the MPB [13]. Additionally, $(Bi_{0.5}Na_{0.5})_{1-x}Ba_xTiO_3$ (BNBT) solid solution from solution precursors with and without $Na^+$ and $Bi^{3+}$ excesses prepared from solution precursors with different concentrations ($x = 0.035$, 0.055, 0.080, 0.100 and 0.150) can be used as a ferroelectric material in future research because of its saturation polarization values and low coercive fields [14]. In vertically aligned nanostructures, there is no such constraint and the ME effect is expected to be stronger. Such a behavior was demonstrated for ferrimagnetic $CoFe_2O_4$ nanopillars embedded in an FE $BaTiO_3$ matrix. Temperature-dependent magnetic measurements demonstrated the coupling between the two-order parameters, which was manifested as a change in magnetization at the FE Curie temperature [15].

Lanthanum doped manganites are intimately related to the coexistence of competing nearly degenerate states which couple simultaneously active degrees of freedom-charge, lattice, orbital, and spin states [16,17]. $La_{0.67}Sr_{0.33}MnO_3$ (LSMO) is considered as a compound with a higher metal-insulator transition temperature and is ferromagnetic at a Curie temperature of 370 K [18]. The electrical and magnetic behavior is largely determined by the electrons in the 3d shell of the manganese atoms [19]. A lot of studies have been

focused on $BaTiO_3$ (BTO) thin films as FE layers because of their remarkable ferroelectric, electrical, optical, nonlinear optical and dielectric properties. Also in their paraelectric and ferroelectric phases offer great promise as capacitor dielectrics for high-density random access memory (RAM) applications. Theoretically, the critical thickness for BTO films has been determined to range from 12 nm to less than 1 nm [20,21]. On $BaTiO_3$ hybridization of d orbitals with occupied p orbitals of the octahedrally coordinated oxygen ions can induce long range polarization [22]. Through its low-temperature structural changes, ferroelectric BTO offers an opportunity to study strain modifications of magnetic and magnetotransport properties [3,4,6,23]. In this work, we investigated the effect of the presence of $BaTiO_3$ layer with different thicknesses ($t_{BTO}$) on structural, electrical and magnetic properties of $La_{2/3}Sr_{1/3}MnO_3/BaTiO_3$ bilayers grown on (001) $SrTiO_3$ substrates by sputtering at high pure oxygen pressures. X-ray diffraction allows to study structural properties, showing a strained LSMO layer and a relaxed behavior on BTO layer. Electrical measurements show a metal behavior at room temperature and magnetic properties like saturation magnetization and coercive field exhibit dependence with BTO thickness.

## 2. Experimental details

LSMO/BTO bilayers were deposited on (001) single-crystal STO by RF and DC sputtering, respectively, at pure $O_2$ pressure around of 3.5 mBar and a substrate temperature of 830°C. A power density of 7 W/cm$^2$ and 12 W/cm$^2$ were used for LSMO and BTO targets, respectively. In our studies, LSMO thickness was chosen around 40 nm and BTO thickness varied in the range from 20 to 100 nm. The thicknesses of the individual layers were obtained by X-ray reflectivity measurements in the bilayers, not shown. X-ray diffraction

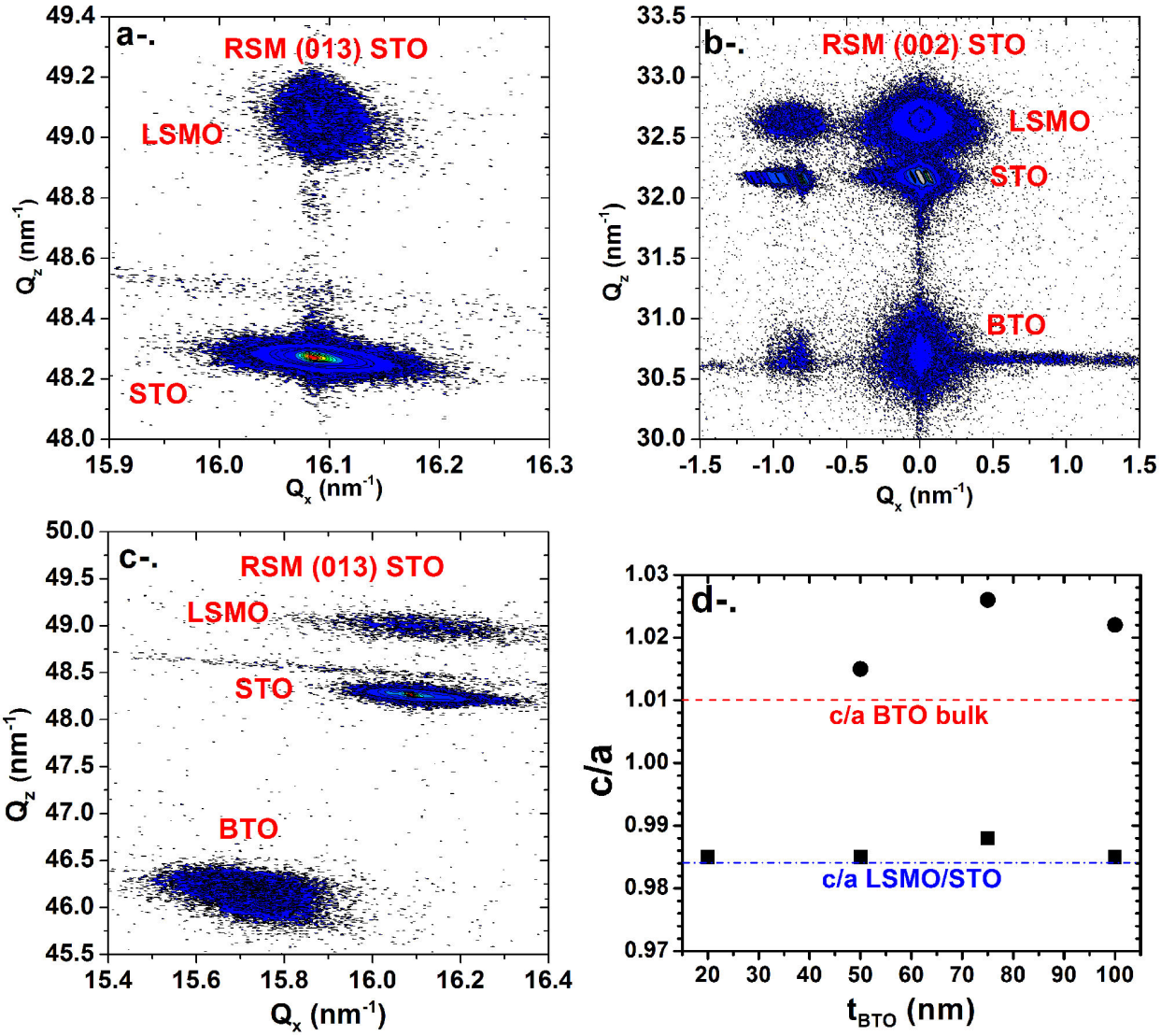


FIGURE 1. a-. Asymmetric (013) RSM for LSMO(40 nm)/STO thin film. b-. Symmetric (002) RSM for LSMO(40 nm)/BTO(20 nm) bilayer. c-. Asymmetric (013) RSM for LSMO(40 nm)/BTO(20 nm) bilayer. d-. c/a ratio dependence with $t_{BTO}$ for all bilayers.

and Reciprocal Space Maps (RMS) measurements show highly textured layers with preferential growth in the c-axis direction. Resistivity as a function of temperature was measured using indium contacts on the surface and aluminum wires (0.127 mm of diameter) with in a current-inplane (CIP) geometry. The magnetic loops, and thermal demagnetization measurements were carried out in a MPMS Quantum Design® system operated by a SQUID detector in the 10-400 K temperature range.

## 3. Results and analysis

### 3.1. Structural properties

In order to determine the degree of relaxation and strain in the bilayers, reciprocal space mapping (RSM) of the bilayers was performed. In Fig. 1a-. (013) asymmetric RSM of LSMO(40 nm)/STO a LSMO film strained is observed, with a lattice parameter c=3.843 Å. For LSMO(40 nm)/BTO(20 nm) bilayer a (002) symmetric RSM show the three materials on Fig. 1b-. Additionally, on (013) asymmetric RSM of LSMO(40 nm)/BTO(100 nm), shown in Fig. 1c, we found a LSMO layer strained due to that on all RSM, the (013) peak of film is aligned with STO peak. Instead of BTO layers is relaxed as is characteristic on all bilayers (in RSM BTO peak is shifted to the left of STO) with a $c/a_{LSMO} = 0.985$ and $c/a_{BTO} = 1.022$. An increase of c/a ratio with $t_{BTO}$ due to BTO relaxation is observed on Fig. 1d-.

### 3.2. CIP transport properties

In Fig. 2 the dependence of resistivity with temperature measured in CIP geometry is shown, for LSMO/BTO with $t_{LSMO} = 40$ nm and varying the thickness of the BTO layer, $t_{BTO}$, from 0 to 100 nm. All bilayers show a metal insulator transition characteristic of the LSMO system above 350 K (not shown). In this system was not observed a weak discontinuity on resistivity, attributed to structural transitions of BTO [5], which was found on LCMO/BTO bilayers due to strain on the interfaces on previous work [5]. The metal insulator transition temperature ($T_{MI}$) is slightly dependent of BTO thickness. A decrease on residual resistivity is observed with increase of $t_{BTO}$, with values near to LSMO/STO thin film 60 $\mu\Omega$cm. The values obtained for the fits are consigned on Table I. At low temperature, the resistivity in zero field was fitted using $\rho(T) = \rho_0 + \rho_2 T^2 + \rho_{4.5} T^{4.5}$, where $\rho_0$ is the residual resistivity, $\rho_2$ is related to electron-electron scattering [24,25] and $\rho_{4.5}$ corresponds to the magnon-magnon scattering [26,27].

### 3.3. Magnetic properties

Figure 3 shows ZFC thermal demagnetization, from 10 to 350 K, for LSMO(40 nm)/BTO ($t_{BTO}$) bilayers, with BTO thickness: 0 nm (diamond), 20 nm (pentagon), 50 nm (triangle), 75 nm (circle) and 100 nm (square). A magnetic field

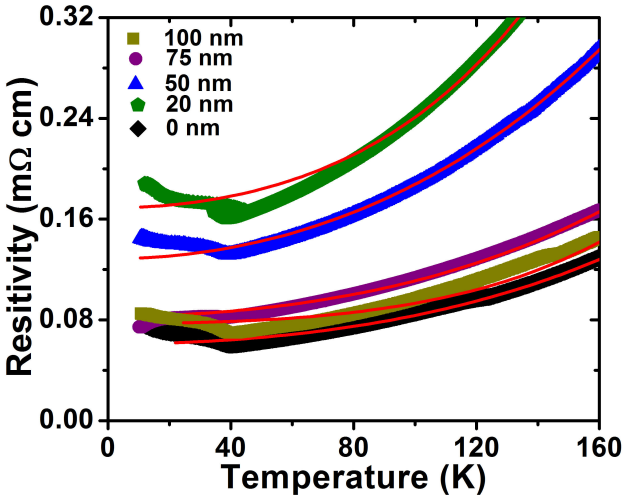


FIGURE 2. Temperature dependence of the resistivity for LCMO/BTO bilayers varying $t_{BTO}$: 0 nm (diamond), 20 nm (pentagon), 50 nm (triangle), 75 nm (circle) and 100 nm (square).

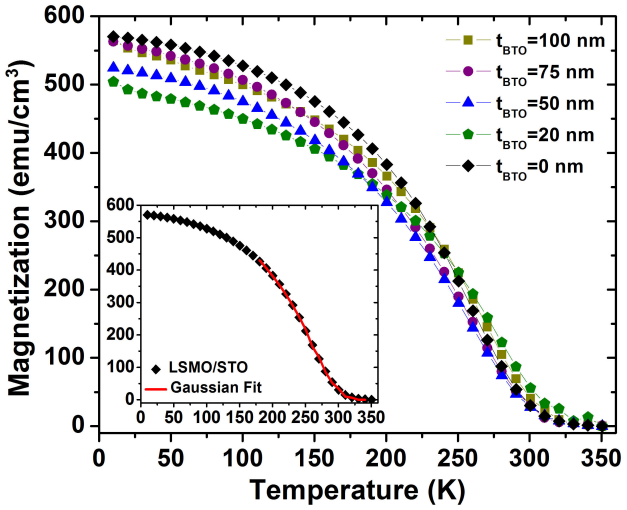


FIGURE 3. Temperature dependence of magnetization at ZFC (Happ = 5 kOe for all bilayers), for LSMO(40 nm)/BTO ($t_{BTO}$)/STO bilayers, with $t_{BTO}$ = 0 nm (diamond), 20 nm (open square), 50 nm (triangle), 75 nm (circle) and 100 nm (square). Inset: Magnetization for LSMO/STO (diamond) with Gaussian fit [28].

TABLE I. Metal insulator transition $T_{MI}$, $\rho_0$, $\rho_2$ and $\rho_{4.5}$ for LSMO/BTO bilayers

| $t_{LSMO}/t_{BTO}$ [nm] | $T_{MI}$ [K] | $\rho_0$ [mΩcm] | $\rho_2\ 10^{-4}$ [mΩcm/K$^2$] | $\rho_{4.5}\ 10^{-11}$ [mΩcm/K$^{4.5}$] |
|---|---|---|---|---|
| 40/0 | 335±2 | 0.06±0.04 | 0.23±0.05 | 1.12±0.02 |
| 40/20 | 306±2 | 0.16±0.07 | 0.72±0.08 | 8.04±0.02 |
| 40/50 | 330±2 | 0.13±0.05 | 0.53±0.07 | 4.28±0.03 |
| 40/75 | 315±3 | 0.08±0.03 | 0.28±0.05 | 2.17±0.04 |
| 40/100 | 320±2 | 0.07±0.05 | 0.24±0.02 | 2.08±0.02 |

TABLE II. Average $T_C$ and Curie temperature distribution width, $\Delta T_C$, for LSMO/BTO bilayers.

| $t_{BTO}$ [nm] | $M_S$ [emu/cm$^3$] | $H_c$ [Oe] | $T_c$ [+1 K] | $\Delta T_c$ [K] | $\beta$ |
|---|---|---|---|---|---|
| 0 | 586±2 | 56±2 | 282 | 48±2 | 0.54±0.02 |
| 20 | 484±2 | 220±2 | 282 | 59±2 | 0.53±0.01 |
| 50 | 534±2 | 178±2 | 282 | 50±2 | 0.50±0.03 |
| 75 | 550±3 | 144±2 | 278 | 53±1 | 0.49±0.02 |
| 100 | 581±2 | 82±2 | 282 | 55±3 | 0.42±0.03 |

($H_{app}$) of 5 kOe was applied parallel to the plane of the film to measure magnetization. By fitting experimental data to a Gaussian distribution of long-range conducting ferromagnetic regions (inset Fig. 3), which has been used in LSMO thin films [28], we extracted Curie temperature, $T_C$, and width of the ferromagnetic/paramagnetic transition temperature $\Delta T_C$ (Table II). Saturation magnetization, coercive field, Curie temperature and $\Delta T_C$ values obtained for an LSMO/STO film and the bilayers grown, are given for comparison. Thermal demagnetization curves display a typical behavior of LSMO thin film. However, LSMO(40 nm) /BTO(50 nm) bilayer (triangle), display the lower Ms$\sim$500 emu/cm$^3$ at 10 K, which is a reduction of 17% on Ms in comparison with LSMO/STO thin film. For other bilayers the reduction on Ms is lower than 10% due to BTO layer influence. In these samples no magnetic moment is blocked or frozen like on previous studies on BTO/LCMO bilayers [6]. The presence of the BTO layer affects the magnetic moment of the ferromagnetic layer at the interface and this interaction depends on the thickness of the BTO layer. Probably, a magnetic contribution exists of the BTO induced by interfacial interactions at the interface, but also induced by crystalline strains originated during the growth process. Critical exponent $\beta$ obtained from fit, identifies a magnetic behavior associated to theoretical model of mean field approximation where $\beta = 0.5$ [29] and was observed on LSMO [30]. In our bilayers, the BTO presence affects $M_s$ and $H_c$ of the LSMO layer. $T_C$ and critical exponents are approximately constant for all bilayers, this may be explained by BTO relaxation observed on RMS. The strain at the interface is not enough for changing the LSMO magnetic mechanism. Additionally, $\Delta T_C$ show that the homogeneity is the same for all bilayers.

Figure 4 shows isothermal magnetic hysteresis loops at 10 K, from -0.6 to +0.6 kOe, for the LSMO(40 nm)/ BTO($t_{BTO}$) bilayers, with BTO thickness. The bilayer exhibit saturation magnetization at magnetic field of 1 kOe. Saturation magnetization in bilayers is lower than that for an LSMO/STO film (590 emu/cm$^3$) grown under identical parameters. Interesting enough, when $t_{BTO}$ reaches 100 nm thick, Ms and Hc (56 Oe) have approximately the same value for a 40 nm thick LSMO film. Figure 5 shows saturation magnetization a-. and coercive field b.- as function of BTO

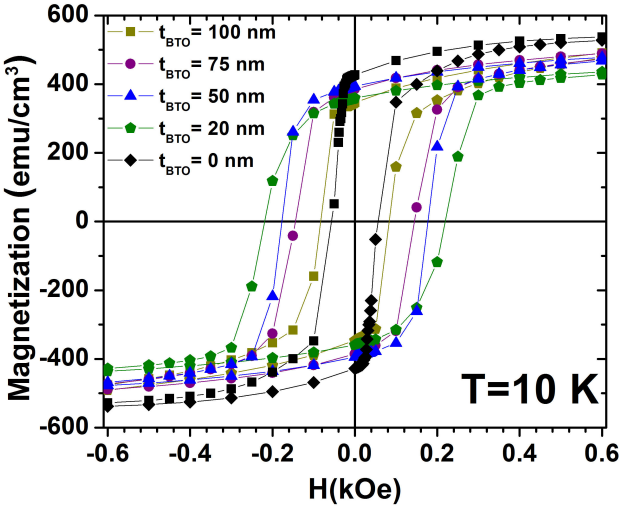


FIGURE 4. Isothermal magnetic hysteresis loops at 10 K for LSMO/BTO bilayers.

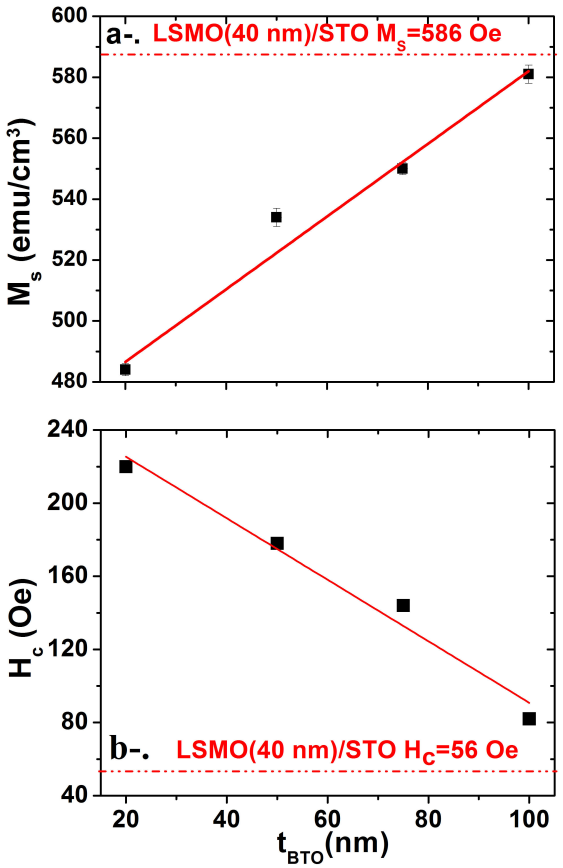


FIGURE 5. BTO layer thickness ($t_{BTO}$) a-. Dependence of saturation magnetization (Circle) and b-. Coercive field (squares). Lines are guides for the eye.

layer thickness, $t_{BTO}$ (nm), where Ms and Hc exhibits a linear behavior. For $t_{BTO}$ smaller than 100 nm Ms is reduced whereas coercive field is bigger than those from the expected value for a film. This reduction of the saturation magnetization and increase of the coercive field in the bilayers could

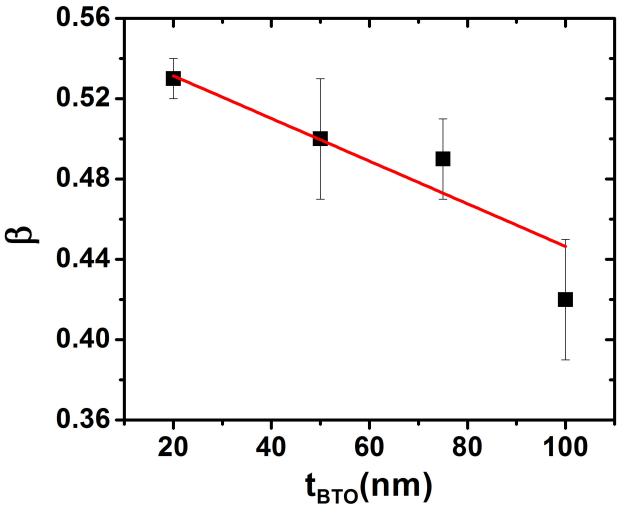


FIGURE 6. Critical exponent $\beta$ dependence with thickness of LSMO thin film.

could be attributed to both spin canting and phase separation at the interface, and strain-induced magnetic disorder in the film [31,32], as we have observed in previous studies on LCMO/BTO and BTO/LCMO [3,4-6]. We observed a dependence of coercive field with $t_{BTO}$. Figure 6 displays de critical exponent dependence with $t_{BTO}$, for bilayers. An apparent change on magnetic mechanism is observed from mean field to near regions of Heisenberg 3d [33-35]. This probably is due to dead layer for low thickness [36,37], and strain on LCMO distorted the MnO octahedral. This dependences confirms the influence of BTO in the magnetic properties of the manganite (for example mismatch LSMO/BTO). In our bilayers magnetic properties of the system are affected by the presence of the ferroelectric layer. Oxygen vacancy can strongly change the correlation effects especially in transition metal oxides. The oxygen vacancies can change the electronic structure; doping with electron/hole; variation in valence of cation; induce local strain; change local electron density; changing the magnetic, dielectric and transport properties of complex metal oxides, also. Additionally, the polarization direction and dislocations on BTO for regions near to interface, can alter the crystalline field and modify the direction of magnetization (from in-plane to out-plane) or cause effects like spin glass, dead layer that alter the magnetism mechanism.

## 4. Conclusions

We studied structural, magnetic and transport properties in ferroelectric/ferromagnetic bilayers of BTO and LSMO oxides grown via DC and RF sputtering in pure oxygen atmosphere, systematically varying the BTO layer thickness and maintaining constant LSMO layer thickness. Bilayers show that LSMO layer is strained on all samples and BTO is always relaxed, c/a ratio (0.986) for LSMO remain approximately constant, while for BTO c/a $> 1$, indicating ferroelectric behavior in this kind of bilayer. Electrical measurements shows that all samples satisfy the electron-electron scattering and magnon-magnon scattering model, so the BTO layer does not affect the electrical transport mechanism in LSMO. The saturation magnetization and coercive field show dependence on BTO thickness, which may be due to relaxation effects of the BTO film for thicker layers.

## Acknowledgments

This work was supported by "Instituto de Nanociencia de Aragón", Zaragoza, Spain, where the films were partially characterized; the Center of Excellence for Novel Materials (CENM); COLCIENCIAS research project: No 110656933104 contract No.2013-0002 CI 7917-CC 10510 COLCIENCIAS-UNIVALLE, "*Study of interface phenomena in hetero-structures based on complex oxides*" CI 7978 and "*Resistive switching in oxides with metal-insulator transitions for applications in random access memories*. CI: 7999" UNIVALLE.

1. L. Martin, Y.-H. Chu, and R. Ramesh, *Mat. Sci. Eng R* **68** (2010) 89-133.
2. E. Dagotto, T. Hott and A. Moreo, *Phys. Rep.* **344** (2001) 1-153.
3. C. Domínguez, J.E. Ordonez, M.E. Gómez and W. Lopera, *J. of Phys.: Conf. Ser.* **480** (2014).
4. J.E. Ordonez, M.E. Gomez, W. Lopera and P. Prieto, *J. Phys.: Conf. Ser.* **614** (2015) 012009.
5. J.E. Ordoñez, M.E. Gomez, W. Lopera and P. Prieto, *J. Phys.: Conf. Ser.* **480** (2014) 1-4.
6. J.E. Ordoñez, M.E. Gomez, W. Lopera and P. Prieto, *IEEE Transactions on Magnetics*, **49** (2013).
7. A. Alberca *et al*., *Phys. Rev. B* **84** (2011) 134402.
8. C. Thiele, K. Dörr, L. Schultz, E. Beyreuther and W.-M. Lin, *Appl. Phys. Lett.* **87** (2005) 162512.
9. C.-G. Duan, S.S. Jaswal, and E.Y. Tsymbal, *Phys. Rev. Lett*. **97** (2006) 047201.
10. J.D. Burton and E.Y. Tsymbal, *Phys. Rev. B* **80** (2009) 174406.
11. Y. Tokura and N. Nagaosa, *Science* **288** (2000) 462-468.
12. E. Dagotto, T. Hott and A. Moreo, *Phys. Rep*. **344** (2001) 1-153.
13. J. Park, E. Vescovo, H. Kim, C. Kwon, R. Ramesh, and T. Venkatesan, *Nature* **392** (1998) 794.
14. P.W. Anderson and H. Hasegawa, *Phys. Rev.* **100** (1955) 675.
15. D.J. Kim *et al*., *Phys. Rev. Lett.* **95** (2005) 237602.
16. R. Nakao, K. Ishizumi, I. Takahashi, H. Terauchi, Y. Hayafuji, and K. Miura, *Appl. Phys. Lett.* **86** (2005) 222901.
17. R.E. Cohen, H. Krakauer, *Phys. Rev. B* **42** (1990) 6416.

18. A. Alberca *et al*., *Phys. Rev. B* **86** (2012) 144416.
19. A. Urushibara *et al*., *Phys. Rev. B* **51** (1995) 14103.
20. G.J. Snyder, R. Hiskes, S. DiCarolis, M.R. Beasley, T.H. Geballe, *Phys. Rev. B* **53** (1996) 14434.
21. K. Kubo and N.A. Ohata, *J. Phys. Soc. Jpn.* **33** (1972) 21-31.
22. S. Mercone *et al*., *Phys. Rev. B* **71** (2005) 064415.
23. A. Berger *et al*.,*J. Appl. Phys*, **91** (2002) 8393-8395.
24. C. Domb, in Phase Transitions and Critical Phenomena, edited by C. Domb and M.S. Green, *Academic, London* **3** (1974) 446-449.
25. M. Ziese, *J. Phys.: Condens. Matter* **13** (2001) 2919-2934.
26. P. Murugavel, and W. Prellier, *J. Appl. Phys.* **100** (2006) 023520.
27. M. Fath *et al*., *Science* **285** (1999) 1540-1542.
28. F. Thorpe, Springer, (2001) pp. 1-309.
29. A. Millis, *Phys. Rev. B* **53** (1996) 8434-8441.
30. P.G. De Genes, *Phys. Rev.* **1** (1960) 118
31. M. Bibes *et al*., *Phys. Rev. Lett.* **87** (2001) 067210.
32. J.Z. Sun, D.W. Abraham, R.A. Rao, and C.B. Eom, *Appl. Phys. Lett.* **74** (1999) 3017.
33. F. Thorpe, Springer, (2001) pp. 1-309.
34. A. Millis, *Phys. Rev. B* **53** (1996) 8434-8441.
35. P.G. De Genes, *Phys. Rev.* **1** (1960) 118.
36. M. Bibes *et al*., *Phys. Rev. Lett.* **87** (2001) 067210.
37. J.Z. Sun, D.W. Abraham, R.A. Rao, and C. B. Eom, *Appl. Phys. Lett*. **74** (1999) 3017.